Embolism resistance of three boreal conifer species varies with pit structure

Uwe G. Hacke[1] and Steven Jansen[2]

[1]Department of Renewable Resources, University of Alberta, 442 ESB, Edmonton, AB T6G 2E3, Canada; [2]Royal Botanic Gardens, Kew, Jodrell Laboratory, Richmond TW9 3DS, Surrey, UK

Author for correspondence:
Uwe G. Hacke
Tel: +1 780 492 8511
Email: uwe.hacke@ualberta.ca

Received: *8 November 2008*
Accepted: *8 January 2009*

New Phytologist (2009) **182**: 675–686
doi: 10.1111/j.1469-8137.2009.02783.x

Key words: bordered pit, embolism resistance, hydraulic conductivity, Pinaceae, torus–margo pit membrane, tracheid, xylem cavitation, wood anatomy.

Summary

• While tracheid size of conifers is often a good proxy of water transport efficiency, correlations between conifer wood structure and transport safety remain poorly understood. It is hypothesized that at least some of the variation in bordered pit and tracheid structure is associated with both transport efficiency and embolism resistance.

• Stem and root samples from three boreal Pinaceae species were collected to test this hypothesis. Tracheid and pit anatomy were studied using light microscopy as well as scanning and transmission electron microscopy.

• While tracheid size explained at least 90% of the variation in specific conductivity for stem and root samples, the strongest correlations with embolism resistance occurred at the pit level. Both torus thickness and depth of the pit chamber showed a linear increase with greater vulnerability to cavitation. Greater embolism resistance was correlated with increasing wood density and tracheid wall reinforcement.

• A thinner torus may be more flexible and better able to seal the pit aperture. The pit chamber depth is proportional to the distance that the margo needs to deflect for pit aspiration.

Introduction

The size of tracheids in conifer xylem varies among species (Bannan, 1965; Panshin & de Zeeuw, 1970; Pittermann *et al.*, 2006a) and within a tree (Bannan, 1965; Rundel & Stecker, 1977; Domec *et al.*, 2006). This variation has important functional implications for water transport. Small increases in the diameter of tracheids can lead to major gains in hydraulic conductivity. When conductivity is expressed on a xylem area basis (specific conductivity, K_S), the Hagen–Poiseuille equation predicts an increase of K_S proportional to the square of the lumen diameter (Tyree & Zimmermann, 2002; Sperry *et al.*, 2006). However, a maximum gain in transport efficiency can only be realized if the end wall conductivity increases in concert with diameter (Lancashire & Ennos, 2002). On its way through the tracheid network, water travels not only through the lumina, but also through the bordered pits of the many thousands of tracheids. The limitation of hydraulic conductivity through pits is influenced by the allometry between tracheid diameter and length. The longer tracheids are, the fewer pits must be crossed, which tends to increase end wall conductivity. Tracheids of most conifers do not exceed a few millimetres in length and are > 10 times shorter than vessels of similar diameter (Pittermann *et al.*, 2005). This explains why end walls account for over 60% of the total resistivity (the inverse of conductivity) in conifer xylem (Domec *et al.*, 2006; Pittermann *et al.*, 2006a), despite the fact that torus–margo pits of conifers offer much higher conductivity than intervessel pits (Pittermann *et al.*, 2005). In the dataset of Pittermann *et al.* (2006a), tracheid length increased in proportion with diameter so that the end wall limitation remained nearly constant. However, more work is necessary to determine whether this is a general pattern in conifer xylem.

While we have learned much about how tracheid size relates to function, less is known about the anatomical adaptations of bordered pits and how they relate to hydraulic characteristics. Embolism resistance, in particular, is thought to be influenced by pit structure. There is considerable support for the air-seeding hypothesis (Tyree & Zimmermann, 2002), which proposes that embolism is caused by air entering a functional conduit from neighbouring air spaces through pores in the conduit wall. Interconduit pit membranes are thought to be important sites of air-seeding (Sperry & Tyree, 1990). Conifer tracheids have

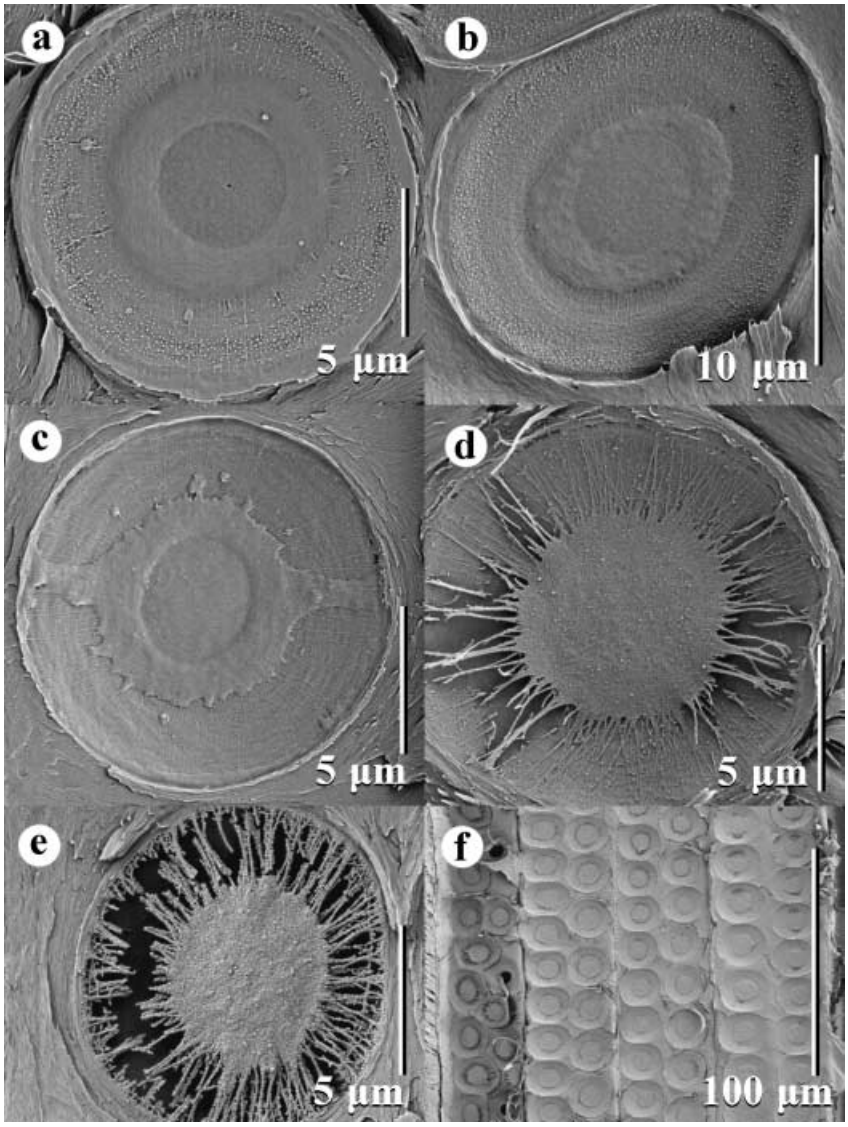

Fig. 1 Scanning electron micrographs of intertracheid pit membranes viewed on radial walls of earlywood in stems (a,c,e) and roots (b,d,f) of three boreal Pinaceae species. Pits tend to be larger in roots than in stems (compare scale bars). When the pit membrane is aspirated (a–c), the aperture outline is visible behind the torus. (a) Circular pit membrane and pit aperture in *Abies balsamea*, warts visible on the pit border. (b) Similar to (a), but with a more oval pit membrane. The upper edge of the torus is close to the edge of the aperture. (c) Aspirated pit membrane with torus straps in *Picea mariana*. (d) Unaspirated pit membrane in *P. mariana*, with some parts of the porous margo broken. (e) Unaspirated pit membrane of *Picea glauca*, showing a granular appearance. (f) Dense packing of pits in earlywood tracheids of roots of *P. glauca*.

pit membranes consisting of a porous margo surrounding a disk-like torus, which represents roughly half of the membrane area (Bauch *et al.*, 1972; Fig. 1). When adjacent tracheids are water-filled, pit membranes are in a relaxed, neutral position while water flows through the large pores of the margo. When an earlywood tracheid embolizes, the pit membranes are deflected to the inside of the pit border and the tori block the pit aperture (Sperry & Tyree, 1990; Domec *et al.*, 2006; Fig. 2d). Nevertheless, the sealing action of the torus has limits. Available evidence suggests that air-seeding in earlywood tracheids may occur when the torus is displaced from its normal sealing position by stretching and possibly rupturing of the margo (Sperry & Tyree, 1990). Air-seeding in torus–margo pits is thought to be a function of the torus overlap (i.e. the relative sizes of pit membrane, torus and pit aperture), the distance the margo must stretch to reach the pit aperture and mechanical properties of margo strands (Sperry & Tyree, 1990; Hacke *et al.*, 2004; Domec *et al.*, 2006; Domec *et al.*, 2008). A recent study on tall Douglas-fir trees reported an increase in the ratio of torus to pit aperture diameter with greater height and greater embolism resistance (Domec *et al.*, 2008). However, such a relationship was not found in the dataset of Hacke *et al.* (2004). Hacke *et al.* (2004) reported that torus diameter increased linearly with increasing pit membrane and pit aperture diameter, which resulted in a fairly narrow range of torus overlap across species. The thickness of the nonporous torus is not known to be related to embolism resistance in conifer wood. It is also unclear whether embolism resistance of conifer xylem is related to the total amount of interconduit pit membrane area per conduit (A_p), as has been proposed for angiosperms (the 'pit area hypothesis', Sperry *et al.*, 2006). This may be expected if intertracheid pits of different species and plant organs provided similar protection from air-seeding and if seeding only occurred as a result of rare structural irregularities. For example, tori and

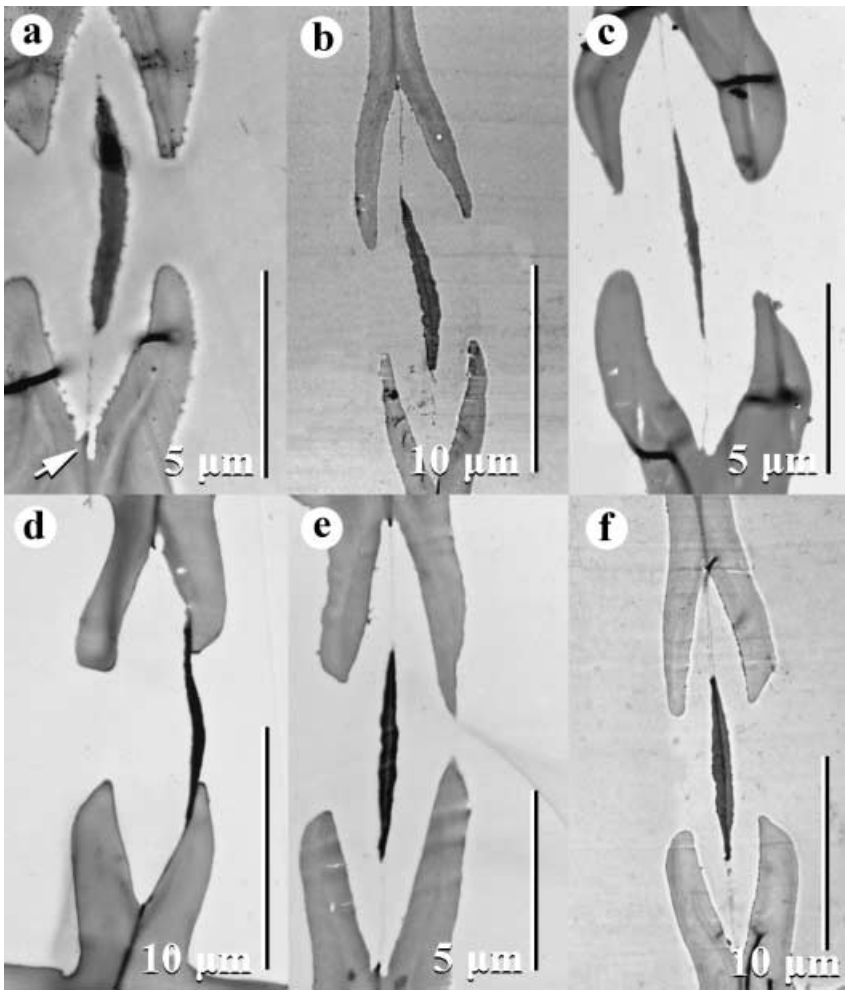

Fig. 2 Transmission electron micrographs of earlywood tracheid pit membranes in stems (a,c,e) and roots (b,d,f) of three boreal Pinaceae species. All pictures show transverse ultrathin (60–90 nm) sections. The pit membranes show a distinct, electron-dense torus and a thin, transparent margo. Pits tend to be larger, with thicker pit membranes, and a deeper pit chamber in roots than in stems. (a,b) *Abies balsamea*. Note the pit membrane annulus (arrow in a) and a dense inner layer of the torus in (b). (c,d) Unaspirated (c) and aspirated pit membrane (d) in *Picea glauca*. (e,f) Pit membranes of *Picea mariana*, showing a more transparent and thinner margo in the stem sample (e) than in the root (f).

pit apertures may not always be perfectly circular, the surface of tori and pit chambers may not always be perfectly smooth, and the margo may occasionally vary in its mechanical properties.

The main goal of this study was to evaluate functional implications of changes in pit anatomy for resistance to embolism and conductivity. Pit ultrastructure was observed with scanning and transmission electron microscopy (TEM). The latter was particularly useful, as it allowed us to evaluate variation in traits that are difficult to study with other methods. Three conifer species that co-occur in the Canadian boreal forest were studied. Only Pinaceae species were selected to minimize phylogenetic constraints on trait variation. In order to include xylem representing a wider range of structural traits and embolism resistance, samples were taken from branches and roots. Roots in conifers are known to be more vulnerable to air-seeding (Sperry & Ikeda, 1997; Kavanagh *et al.*, 1999; Hacke *et al.*, 2000) and tend to show higher conductivities than branches (Kavanagh *et al.*, 1999; Domec *et al.*, 2006; Pittermann *et al.*, 2006b).

We hypothesized that the average tracheid diameter (D) of a xylem sample will be correlated with average tracheid length (L), allowing a proportional increase of K_S with D. Assuming that pit membranes are the sites of air-seeding, we also hypothesized that embolism resistance will vary more with pit ultrastructure than with tracheid dimensions. In particular, we tested whether the ratio of torus to pit aperture diameter was correlated with embolism resistance, as reported for Douglas-fir trees (Domec *et al.*, 2008). We also tested whether the pit area hypothesis applies for the conifer species studied. Finally, we hypothesized that embolism resistance will be correlated with wood density and tracheid wall reinforcement, as shown in previous studies (Hacke *et al.*, 2001; Hacke *et al.*, 2004).

Materials and Methods

Plant material

Branches and roots of *Picea glauca* (Moench) Voss and *Abies balsamea* (L.) Mill. were collected from the University of Alberta's Woodbend field station, located 25 km southwest of Edmonton, Canada (53°25′N, 113°45′W, elevation 700 m). Trees were 1.5–2 m tall and were growing in sandy soil. *Picea mariana* (Mill.) BSP. was gathered from a peat bog *c.* 20 km east of Edson, Alberta. Trees were mature and growing in association with *Larix laricina* (Du Roi) K.Koch. Plant material was brought

to the laboratory in moist plastic bags. All hydraulic measurements (below) were conducted within 4 d after sampling.

Hydraulic conductivity and embolism resistance

Branch and root segments were cut under water. Segments had a length of 14.5 cm and a diameter (including bark) of 4–8 mm and 7–10 mm for roots and branches, respectively. The same segments were used for all hydraulic and anatomical measurements. A set of three segments was measured per species and organ. Segments were trimmed with new razor blades to a final length of 14.2 cm. For stems, *c.* 2 cm of the bark was removed at both ends of the segment to prevent the accumulation of excess resin. The segments were then flushed with 20 mM KCl + 1 mM $CaCl_2$ solution (van Ieperen & van Gelder, 2006) at 10 kPa for 30 min to remove reversible embolism. A low water pressure was used for flushing to prevent pit aspiration. Native embolism was minimal. The deionized water for this solution had been filtered through an E-Pure system (Barnstead, Dubuque, IA, USA) and a capsule filter (0.2 μm). The segments were then fitted to a tubing apparatus (Sperry *et al.*, 1988) where the initial hydraulic conductivity was measured, using the same solution that was used for flushing. Hydraulic conductivity was calculated as the quotient of flow rate through the segment and pressure gradient along the segment. Conductivity was based on the net flow rate through a segment. The net flow rate was determined by measuring the total flow under a pressure of 4–5 kPa and subtracting the 'background' flow, measured in the absence of a difference in hydraulic head across the segment. Background flow was measured before and after the pressurized flow, with the average used to calculate the net flow. Each flow measurement was the average of five successive 10-s measurements and was monitored gravimetrically using an electronic balance (CP225D; Sartorius, Göttingen, Germany) interfaced with a computer using COLLECT 6 software (Labtronics, Guelph, Canada). Conductivity was corrected to 20°C to standardize for temperature-dependent viscosity effects. The maximum hydraulic conductivity was used to determine the specific conductivity (K_S), which is the hydraulic conductivity per transverse sectional xylem area (Tyree & Zimmermann, 2002). Xylem area was determined from a cross-section through the middle of a segment. The area was measured with a stereomicroscope (MS5; Leica Microsystems, Wetzlar, Germany) equipped with a digital camera (Infinity 1; Lumenara, Ottawa, Canada) and interfaced with a computer for image analysis.

Vulnerability curves were generated to evaluate the xylem's resistance to embolism. The centrifuge method was used (Alder *et al.*, 1997). Segments were spun in a custom-built rotor to increasingly negative xylem pressures. Segments were held at each target pressure for 10 min to ensure complete embolism before being taken out of the rotor, and before hydraulic conductivity was measured again. The percentage loss in conductivity from the original value was plotted versus the negative pressure, and curves were fitted with a Weibull function. The xylem pressure corresponding to 50% loss of conductivity (P50) was calculated for each segment.

Tracheid dimensions and pit area

Transverse sections were prepared with a sliding microtome or with razor blades. Sections were stained with toluidine blue for 3 min, rinsed in water, and mounted on glass slides with glycerine. Photographs of the outer two growth rings were taken at 200× magnification with a Leica DFC420C digital camera mounted on a DM3000 microscope (Leica Microsystems). Lumen diameters were measured in a minimum of three radial sectors encompassing earlywood and latewood as well as normal and compression wood. Diameters were measured with an image analysis program (IMAGEPRO PLUS 6.1; Media Cybernetics, Silver Spring, MD, USA). The mean tracheid diameter of a stem or root segment was calculated from a minimum of 200 tracheids. Based on the Hagen–Poiseuille equation, the diameter of the average tracheid of a segment was calculated as $D = [(\Sigma d^4)/n]^{1/4}$ (n is the number of tracheids measured and d is the individual lumen diameter). Hence, D represents the diameter of a tracheid of average lumen conductivity (Tyree & Zimmermann, 2002; Wheeler *et al.*, 2005). The hydraulic mean diameter (d_h) was also calculated from the same tracheid diameter distributions used to obtain D. It was calculated as $d_h = \Sigma d^5/\Sigma d^4$ and was required to measure the thickness-to-span ratio (see below). Tracheids of this diameter will embolize at P50 if air-seeding progresses from wide to narrow tracheids, which is observed within a sample (Hacke *et al.*, 2001).

Tracheid length was measured on individual tracheids obtained from macerations. After the bark was removed, small pieces of wood were cut from the outermost growth rings of a segment. These pieces included earlywood and latewood, and were digested in a 1 : 1 solution of glacial acetic acid and 30% hydrogen peroxide for 48 h at 60°C (Chaffey, 2002). The samples were then rinsed in water, stained with toluidine blue for 3 min and mounted on glass slides with water. Micrographs were taken using a light microscope at low magnification or a stereomicroscope (same equipment as described above), and tracheid length was measured using IMAGEPRO PLUS. A minimum of 100 tracheids was measured per stem or root segment to obtain the average tracheid length per segment (L).

The average tracheid area (A_T) was calculated as $4DL$, where D is the width of one side of a tracheid, assuming a square transverse tracheid shape (Pittermann *et al.*, 2006a; Hacke *et al.*, 2007). The intertracheid pit area (A_p) was estimated from the same macerations used to measure L. The A_p was calculated from $A_p = A_T F_p$, where F_p is the average fraction of the tracheid wall area occupied by intertracheid pits (Pittermann *et al.*, 2006a). The F_p was measured on sequential photographs of complete radial walls of earlywood tracheids taken at 200× magnification. The intertracheid pit area (= pit membrane area) on one complete radial wall was measured with the tracing function of the image analysis software. The fraction was divided

by two to account for nonpitted tangential walls. A segment's mean F_p was calculated from measurements on at least five complete earlywood tracheids.

Mechanical properties

Tracheid 'thickness-to-span ratios', $(t/b)_h^2$, were used as anatomical proxies for tracheid wall reinforcement. The t represented the tracheid double wall thickness and was measured as described previously (Hacke *et al.*, 2001, 2004; Pittermann *et al.*, 2006b). The width of the wall (b) was calculated as the side of a square with an area equal to the area of the tracheid lumen (Hacke *et al.*, 2004). For the rectangular shape of tracheids, this was a better approximation than setting $b = d_h$, as is typically done for vessels. For each segment, the $(t/b)_h^2$ was measured on 20–30 tracheids whose lumen diameters were within ± 2 μm of d_h. Wall thickness was measured on tangential walls that did not contain pits. To determine whether resistance to embolism increases with wood density, the dry weight per fresh volume of wood samples was measured. One *c.* 2-cm long wood sample was prepared per segment and was cleaned of any pith and bark material. The sample was submerged in water to measure its volume displacement. The displacement weight was converted to sample volume. Samples were subsequently dried at 70°C for 3 d and their dry weight was measured.

Electron microscopy

A fresh sample 1 cm long was cut from each of nine stem and eight root segments, put in a zipseal bag with wet paper towels, and express-shipped to the Royal Botanic Gardens, Kew, UK. At Kew, 17 samples (five samples for *A. balsamea* and six samples for *P. glauca* and *P. mariana* each) were prepared for scanning electron microscopy (SEM) and TEM. The SEM samples were cut into 5–10 mm lengths, split in half and dehydrated in an ethanol series of 50, 70, 95 and 100% for 5 min in each solution. Samples were then air dried for 12 h at room temperature and split in the tangential or radial plane. The split samples were fixed to aluminium stubs with electron conductive carbon cement (Neubauer Chemikalien, Münster, Germany) and coated with platinum using an EMITECH K550 sputter coater (Emitech Ltd, Ashford, UK) for 2 min. Samples were observed with a Hitachi S-4700 field-emission scanning electron microscope (Hitachi High Technologies Corp., Tokyo, Japan) at an accelerating voltage of 2 kV. The TEM samples were cut into 2 mm^3 blocks and fixed overnight in Karnovsky's fixative at room temperature. After washing in a 0.05 M phosphate buffer, the specimens were postfixed in 1% buffered osmium tetroxide for 4 h at room temperature, washed again, and dehydrated through a graded ethanol series (30, 50, 70, 90 and 100%). The ethanol was gradually replaced with LR White resin (London Resin Company, Reading, UK) over several days, with the resin being changed approximately every 12 h. The resin was polymerized in a Gallenkamp vacuum oven at 60°C and 1000 mbar for 24 h. Embedded samples were trimmed with a Leica EM specimen trimmer (Leica Microsystems) and sectioned on an ultramicrotome (Ultracut; Reichert-Jung, Vienna, Austria). Sections of 1 μm and 2 μm were cut with a glass knife, heat-fixed to glass slides, stained with 0.5% toluidine blue O in 0.1 M phosphate buffer, and mounted in DPX (Agar Scientific, Stansted, UK). Resin-embedded material was prepared for TEM-observations by cutting ultrathin sections between 60 nm and 90 nm using a diamond knife. The sections were attached to Formvar grids (Agar Scientific) and stained with uranyl acetate and lead citrate using a Leica EM Stain Ultrostainer (Leica Microsystems). Observations were carried out using a JEM-1210 TEM (Jeol, Tokyo, Japan) at 80 kV accelerating voltage and digital images were taken using a MEGAVIEW III camera (Soft Imaging System, Münster, Germany).

Pit dimensions

The dimensions of individual intertracheid pits were evaluated on earlywood tracheids based on electron microscopy photographs. Measurements included the diameter of the pit membrane (D_M), the torus diameter (D_T) and the pit aperture diameter (D_A). These parameters were measured based on a total of 130 SEM and 118 TEM micrographs. The TEM photographs showed cross-sections of pit pairs. When such sections were observed, the aperture sizes of a pit pair differed occasionally (Fig. 2e). In those cases, the larger of the two pit apertures was measured. Cross-sections will only show the maximum D_T and D_A if the pit is cut in its centre. Otherwise, values will underestimate the actual diameters. The deviation will be largest for D_A because of its small size. For that reason, measurements on transverse sections of pit pairs were compared with SEM photographs depicting face views of pits. In many cases, pits were aspirated, and D_M, D_T and D_A could be viewed on the same pit, because the aperture outline could be traced behind the aspirated torus (Fig. 1a,c). When the aperture was not visible behind the torus, only D_M and D_T could be measured on the same pit. In other cases, the pit membrane including torus was removed by the sample preparation so that only D_M and D_A could be measured on the same pit. Based on TEM photographs, the maximum torus thickness was measured as well as the maximum distance between the overarching pit borders (measured in perpendicular direction to the pit membrane). The latter parameter defines the depth of the pit chamber and the distance the membrane deflects before aspiration occurs. The depth of the pit chamber could be determined on both sides of the aperture. When the distance was different on both sides, the longer distance was measured. All measurements were conducted with IMAGEPRO PLUS software.

Evaluating linear relationships

All correlations were evaluated with standardized major axis (SMA) slope-fitting, because we were interested in estimating

the scaling best describing the bivariate scatter of the variables, instead of predicting the value of one variable from another. Regression slopes were calculated using the computer package SMATR 2.0 (Warton *et al.*, 2006).

Results

General pit micromorphology

Pit membranes were often aspirated in SEM micrographs (Fig. 1a–c). Warts between 30 nm and 80 nm in diameter were distinctly associated with the pit border in *A. balsamea* and showed a higher density towards the rim of the pit border than near the aperture (Fig. 1a,b). Pit borders in *P. glauca* and *P. mariana* were fairly smooth and free of warts. The shape of the pit aperture and torus was mostly circular to oval (Fig. 1a,b), although a more irregular shape of the torus was found in several pits. All samples studied showed a well-defined torus (i.e. an electron-dense central area of the pit membrane) in their earlywood tracheids (Fig. 2). The TEM micrographs frequently revealed an inner layer of the torus, which is either electron denser (Fig. 2b,f) or brighter (Fig. 2e), than the rest of the torus. An annulus (Fig. 2a,e) occurred near the rim of pit borders and was slightly more distinct in stem material than in root samples. The torus occasionally showed thickening bars ('margo straps') radiating entirely or partly from the torus to the margo periphery in all three species (Fig. 1c). Similarly, granular structures interwoven in the microfibrillar network of the margo occurred sporadically (Fig. 1a,c). The torus was usually smooth in appearance (Fig. 1a–c), but sometimes slightly granular in the two species of *Picea* (Fig. 1d,e).

Structure–function relationships at the pit level

The interspecific variation in quantitative pit characteristics was less significant than the differences found between root and stem material within a single species. The pit membrane diameter was significantly larger in roots than in stem material (mean ± SD of eight root and nine stem samples: 17.7 ± 1.3 μm vs 11.6 ± 1.0 μm, respectively; Figs 1a,b, 2). While pitting in stem tracheids was predominantly uniseriate, biseriate pitting frequently occurred in radial walls of root tracheids (Fig. 1f). Compared with stems, roots also showed higher values for D_T (mean ± SD: 8.4 ± 0.7 μm in roots vs 5.7 ± 0.6 μm in stems), D_A (mean ± SD: 4.8 ± 0.7 μm in roots vs 2.9 ± 0.5 μm in stems), torus thickness, margo thickness (average values from 170 to 220 nm in roots vs 120 to 150 nm in stems) and pit chamber depth.

Torus diameter increased linearly with pit membrane diameter (Fig. 3, triangles). This was observed in cross sections of pit pairs (grey triangles, $R^2 = 0.86$) and in surface views of pits (black triangles, $R^2 = 0.89$). The regression lines had a common slope, regardless of whether the dimensions were measured from cross sections (with TEM) or surface views of pits (with SEM).

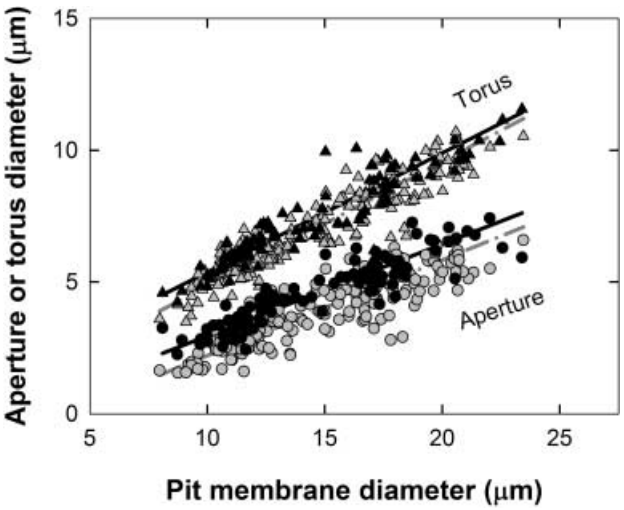

Fig. 3 Torus (D_T, triangles) or pit aperture (D_A, circles) diameter vs pit membrane diameter (D_M) for pooled root and stem tracheids. Measurements were either done on surface views of pits (closed symbols and solid lines) or on cross sections of pits (tinted symbols and dashed lines). The standardized major axis (SMA) regression lines are shown for pooled stem and root data. All regressions had high coefficients of determination ($R^2 \geq 0.86$ for D_T vs D_M scaling, $R^2 \geq 0.75$ for D_A vs D_M scaling) and were highly significant ($P < 0.001$). The common slope was 0.46 for the D_T vs D_M relationship and 0.36 for the D_A vs D_M relationship.

However, there was a significant ($P < 0.001$) shift in elevation between the two groups. The D_T as measured on surface views of pits was larger at a given D_M than the D_T measured in cross-sections. Similar results were obtained for the scaling of D_A with D_M (Fig. 3, circles). The slopes of the regression lines were the same for SEM and TEM, but aperture diameters were larger ($P < 0.001$) when measured in surface views. This is consistent with the fact that surface views always allowed the determination of maximum diameters, whereas this was not necessarily the case in cross-sections.

Across all samples, the ratio of torus to pit aperture diameter increased linearly with increasing resistance to embolism (Fig. 4a). This was accompanied by an increase in the ratio of pit membrane to pit aperture diameter (Fig. 4b). However, for a given torus–aperture ratio, the air-seeding pressure spanned a range of > 2 MPa. Stronger anatomical correlates with P50 on the level of individual pits are shown in Fig. 5. Torus thickness increased linearly with greater vulnerability (Fig. 5a). This trend was paralleled by an increase in the maximum distance between pit borders (i.e. the pit chamber depth) with increasing vulnerability (Fig. 5b). Root samples tended to have thicker tori and deeper pit chambers than stem samples. Specific conductivity increased with increasing D_M and D_A (Fig. 6a) as well as D_T (data not shown). Specific conductivity showed weaker positive correlations with pit chamber depth (Fig. 6b) and torus thickness (data not shown). There was no correlation between K_S and the torus–aperture or the pit membrane–aperture ratio.

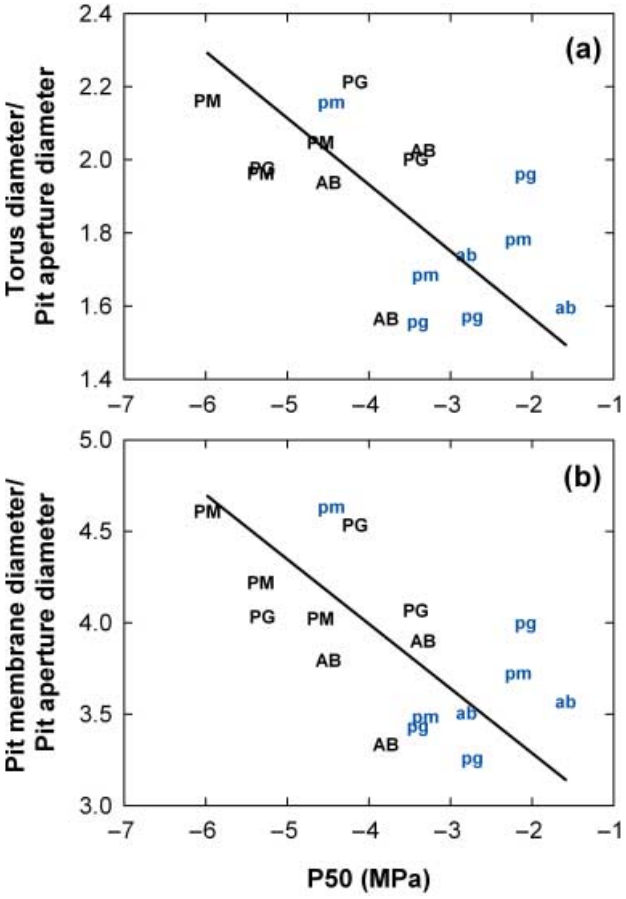

Fig. 4 The ratio of torus to pit aperture diameter (a) increased with embolism resistance, expressed as P50 ($R^2 = 0.34$, $P = 0.01$). This was paralleled by an increase in the ratio of pit membrane to pit aperture diameter (b) with greater embolism resistance ($R^2 = 0.37$, $P = 0.01$). Lower case letters, roots; upper case letters, stems. Species abbreviations: AB/ab, *Abies balsamea*; PG/pg, *Picea glauca;* PM/pm, *Picea mariana*.

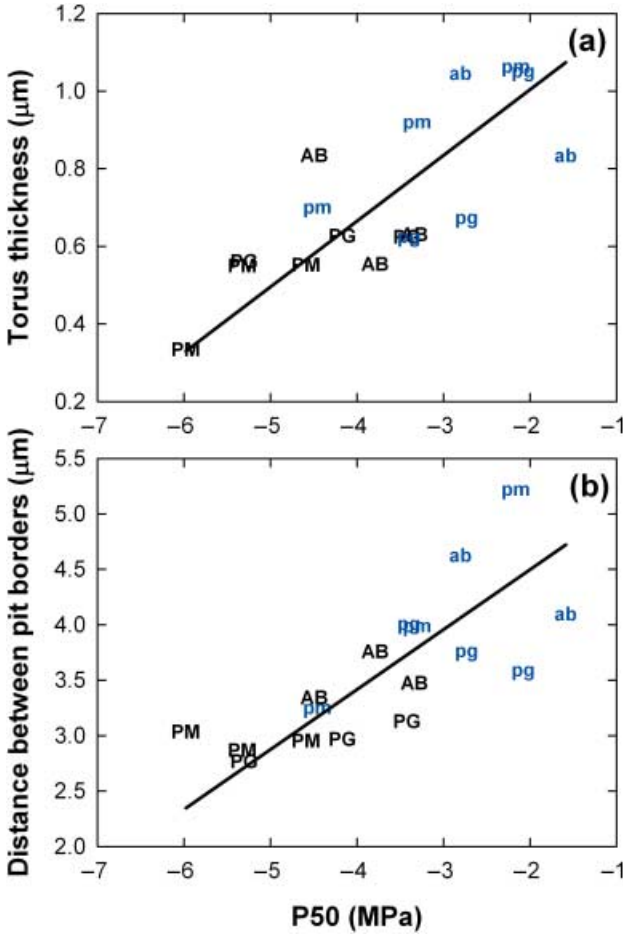

Fig. 5 (a) Torus thickness increased with greater vulnerability to embolism ($R^2 = 0.56$, $P = 0.001$). The distance between pit borders (b) showed a similar increase with xylem vulnerability ($R^2 = 0.56$, $P = 0.001$). Lower case letters, roots; upper case letters, stems. Species abbreviations: AB/ab, *Abies balsamea;* PG/pg, *Picea glauca*; PM/pm, *Picea mariana*.

Structure–function relationships at the tracheid and tissue level

Roots and stems showed very different relationships between tracheid dimensions and embolism resistance. In roots, tracheid diameter decreased with greater resistance to embolism, but there was no significant correlation in stems (Fig. 7a). A similar trend existed with regard to tracheid length (Fig. 7b). In roots, longer tracheids tended to be more vulnerable. There was no correlation between L and P50 in stem samples. Following the trends seen for D and L, tracheid area decreased with greater embolism resistance (Fig. 7c). This trend occurred in roots and stems. Both SMA regression lines had a common slope (−0.86), but there was a shift in elevation between groups. The pit area of root samples was correlated with embolism resistance, but there was no correlation among stem samples (Fig. 7c). Tracheids in roots showed much higher intertracheid pit area than stem tracheids. This was because of the greater surface area of root tracheids and the fact that the wider tracheids of roots tended to have higher pit fractions than stem tracheids. The mean pit fraction was 13.3 ± 2.4% (± SD) for roots and 9.6 ± 0.7% for stems. Greater embolism resistance was also correlated with increasing wood density (Fig. 8a) and thickness-to-span ratio (Fig. 8b).

Differences in tracheid anatomy were closely linked with variation in K_S. Tracheid diameter and length increased with increasing K_S (Fig. 9a,b), as did tracheid area (Fig. 9c). Tracheids in roots were wider and longer and consequently had greater surface area than tracheids in stems. The particularly tight correlation between K_S and A_p (Fig. 9c, $R^2 = 0.95$) agrees with pits representing a major resistance to water flow. Average tracheid length scaled with tracheid diameter (Fig. 10). The slope of the SMA regression line was 0.77.

Discussion

Detailed anatomical observations of pit and conduit dimensions based on light microscopy (LM), SEM and TEM in

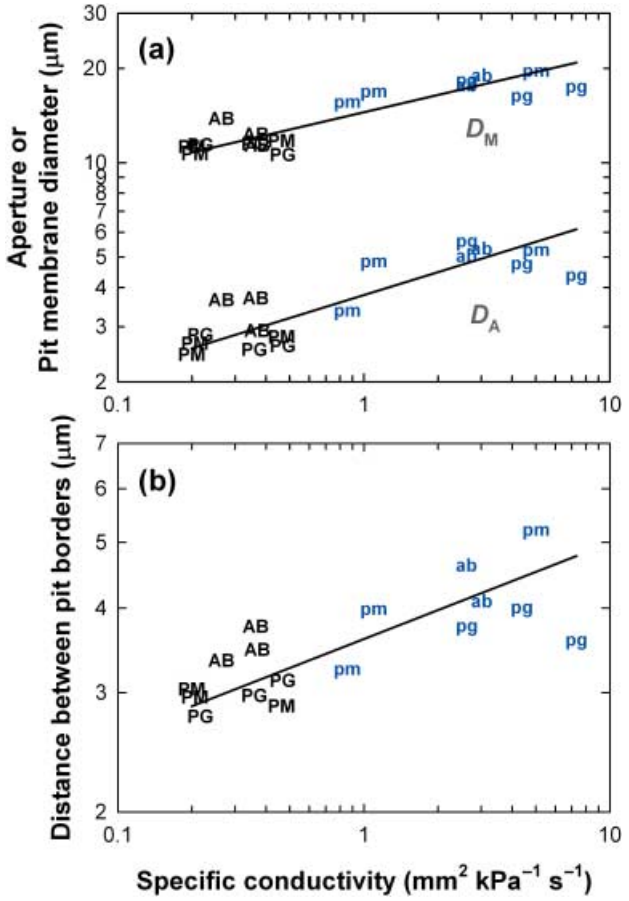

Fig. 6 Log–log plots showing relations between pit structure and specific conductivity. (a) Increase of pit membrane diameter ($R^2 = 0.80$, $P < 0.001$) and pit aperture diameter with specific conductivity ($R^2 = 0.72$, $P < 0.001$). (b) The distance between pit borders also showed a positive correlation with specific conductivity ($R^2 = 0.59$, $P < 0.001$). Lower case letters, roots; upper case letters, stems. Species abbreviations: AB/ab, *Abies balsamea*; PG/pg, *Picea glauca*; PM/pm, *Picea mariana*.

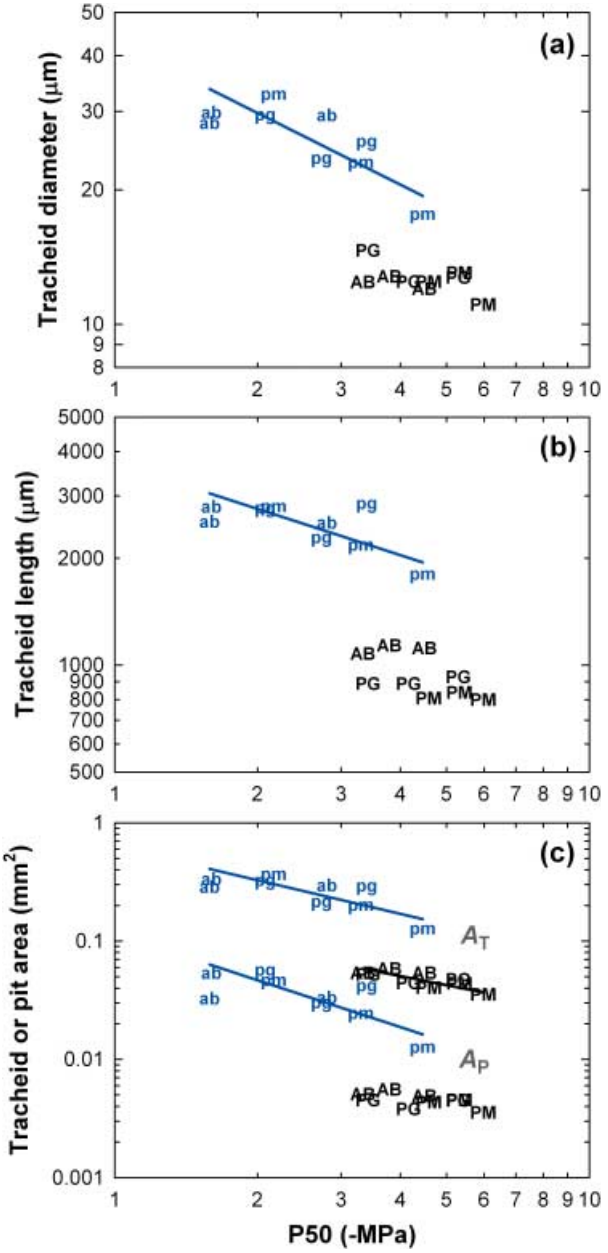

Fig. 7 Log–log plots showing relations between tracheid dimensions and resistance of xylem to embolism, expressed as P50 (50% loss of conductivity). The P50 is shown in absolute values for log transformation. (a) Average tracheid diameter in relation to P50. A correlation existed among root samples (lower case letters; $R^2 = 0.59$, $P = 0.02$), but not among stem samples (upper case letters; $P = 0.11$). (b) Average tracheid length in relation to P50. The correlation was marginally significant among root samples ($R^2 = 0.44$, $P = 0.053$), but not in stems ($P = 0.12$). Stem tracheids were much shorter than root tracheids at a given P50. (c) Average tracheid area (A_T) and intertracheid pit area (A_P) vs P50. The A_T decreased in roots ($R^2 = 0.55$, $P = 0.02$) and stems ($R^2 = 0.55$, $P = 0.02$) with increasing embolism resistance, but stem tracheids had a significantly smaller surface area per embolism pressure than tracheids in roots ($P < 0.001$). In roots, the A_P decreased with embolism resistance ($R^2 = 0.51$, $P = 0.03$), but there was no correlation in stems ($P = 0.12$). Lower case letters, roots; upper case letters, stems. Species abbreviations: AB/ab, *Abies balsamea*; PG/pg, *Picea glauca*; PM/pm, *Picea mariana*.

combination with measurements of hydraulic efficiency and safety offer interesting new ways to investigate functional implications of micromorphological variation associated with water conductive cells. Bordered pits and pit membranes seem to provide ideal structures for such an interdisciplinary approach because of their small size and significant role in xylem transport. Scanning electron microscopy and TEM techniques allow us to measure structural traits of bordered pits with greater accuracy than studies that rely on LM (Hacke *et al.*, 2004; Pittermann *et al.*, 2006a). Moreover, it seems important to use the same plant material for both hydraulic measurements and anatomical observations because there is considerable evidence of intraspecific variation in wood anatomy and phenotypic plasticity in hydraulic conductivity and P50 values (Cochard *et al.*, 1999; Tyree & Zimmermann, 2002). While considerable attention has been paid to the ultrastructure and development of bordered pits in conifers (Bauch *et al.*, 1972; Dute *et al.*, 2008), the

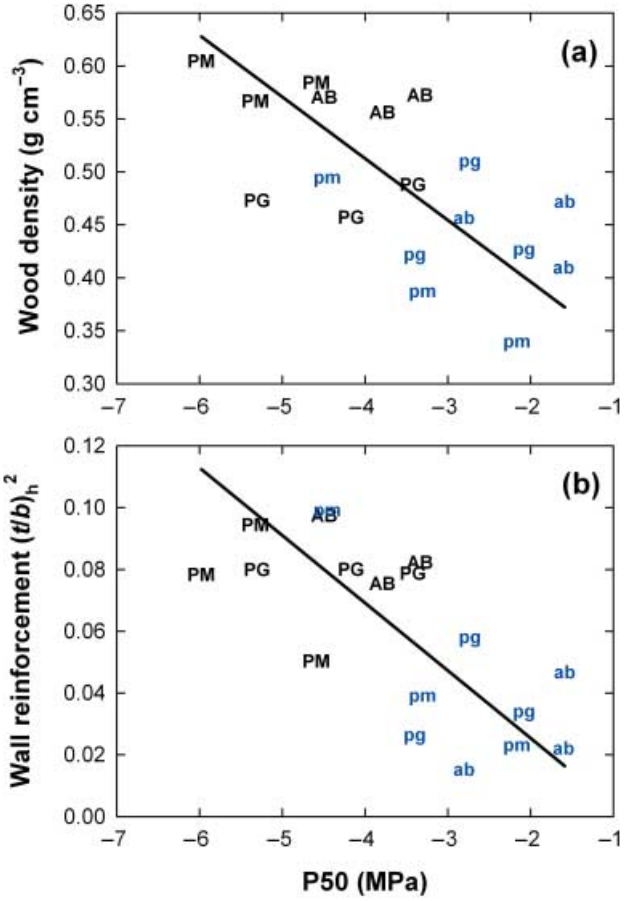

Fig. 8 Increase of wood density (a) and thickness-to-span ratio (b) with increasing embolism resistance. In both cases, correlations were highly significant for pooled stem and root samples ($R^2 = 0.42$, $P = 0.004$ for wood density; $R^2 = 0.51$, $P = 0.001$ for thickness-to-span ratio). Lower case letters, roots; upper case letters, stems. Species abbreviations: AB/ab, *Abies balsamea;* PG/pg, *Picea glauca*; PM/pm, *Picea mariana*.

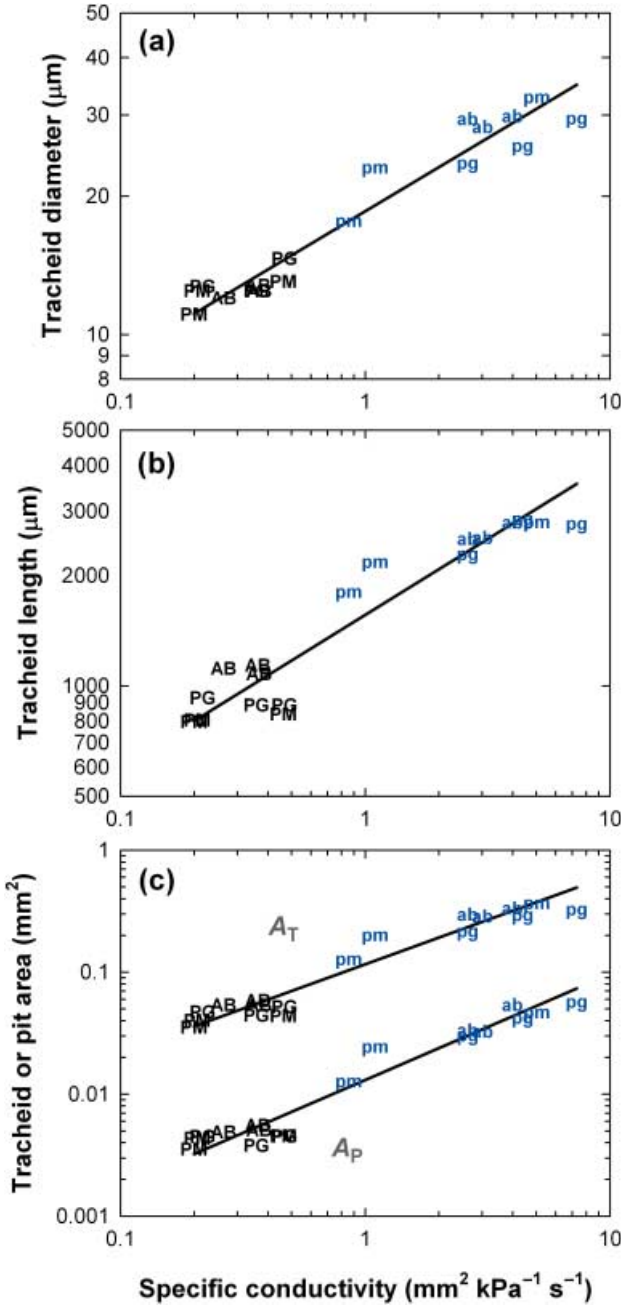

Fig. 9 Log–log plots showing relations between tracheid dimensions and specific conductivity (K_S) of the xylem. (a) Average tracheid diameter in relation to K_S ($R^2 = 0.94$, $P < 0.001$). The standardized major axis (SMA) regression line for pooled stem and root samples has a slope of 0.32. (b) Average tracheid length in relation to K_S ($R^2 = 0.90$, $P < 0.001$). The SMA regression line has a slope of 0.41. (c) Average tracheid area (A_T, $R^2 = 0.94$, $P < 0.001$) and intertracheid pit area (A_P, $R^2 = 0.95$, $P < 0.001$) versus K_S. The SMA regression lines for pooled stem and root samples have a slope of 0.73 (A_T vs K_S) and 0.87 (A_P vs K_S). Lower case letters, roots; upper case letters, stems. Species abbreviations: AB/ab, *Abies balsamea*; PG/pg, *Picea glauca*; PM/pm, *Picea mariana*.

application of SEM and TEM techniques to xylem hydraulic measurements in plants remains relatively unexplored (Jansen *et al.*, 2009). Gaps in understanding the function of bordered pits arise from the need to integrate structural aspects with physiological measurements of pit membrane resistance, embolism resistance and water flow efficiency. Understanding which anatomical parameters at the cell and tissue level are most closely correlated with hydraulic safety and efficiency traits could be useful to test structure–function hypotheses on a larger number and broader taxonomic range of species. Ideally, these general traits should also be evaluated in an evolutionary and ecological context. This argues for an interdisciplinary approach and close collaboration between different research areas when aiming to confront recent issues related to embolism resistance and functional wood anatomy.

Use of electron microscopy revealed strong scaling relationships between torus and pit membrane diameters (Fig. 3). The

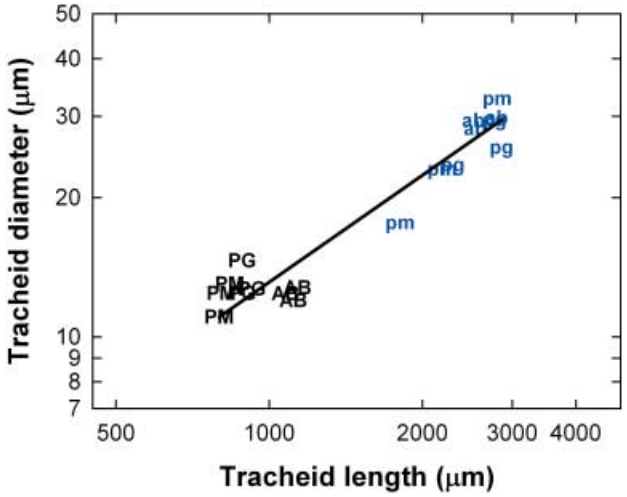

Fig. 10 Log–log plot showing allometric scaling of tracheid diameter and tracheid length ($R^2 = 0.93$, $P < 0.001$). The slope of the standardized major axis (SMA) regression line for pooled stem and root samples was 0.77. Lower case letters, roots; upper case letters, stems. Species abbreviations: AB/ab, *Abies balsamea*; PG/pg, *Picea glauca*; PM/pm, *Picea mariana*.

torus represented *c*. 48% of the pit diameter, which is similar to the 49% reported by Hacke *et al.* (2004) and the 45% found in earlywood tracheids of Douglas-Fir (Domec *et al.*, 2006). Pit aperture also increased linearly with the diameter of the pit membrane. This tight scaling of pit dimensions across species and organs is likely to have important functional implications and highlights the putative role of intertracheid pits in constraining both hydraulic efficiency and safety from embolism. Variation in torus diameter relative to D_M and D_A can be described by the torus overlap $[(D_T - D_A)/(D_M - D_A)]$, which is the fraction of the pit border width that is covered by the torus. In our dataset this parameter varied between 0.23 and 0.35 with a mean of 0.30 ± 0.04 (± SD). This is similar to the range observed by Hacke *et al.* (2004) and agrees with predictions of their model. According to the model of Hacke *et al.* (2004), maximum pit conductivity occurs for a torus overlap of between 0.24 and 0.30. While a smaller torus would allow for greater margo area, it would require more margo spokes to prevent the torus from being displaced from its sealing position and to prevent the xylem from becoming more vulnerable to air-seeding. This would reduce the porosity of the margo and hence conductivity. A torus wider than the optimum reduces the margo area, which will also reduce pit conductivity. Based on our data set, there was no correlation between the torus overlap as defined by $(D_T - D_A)/(D_M - D_A)$ and P50 ($P = 0.07$), but there was a weak correlation between the ratio of torus to pit aperture diameter and embolism resistance (Fig. 4a). Roots tended to show smaller ratios than stems. However, this trend was more pronounced within tall Douglas-fir trees, where it appears to play an important role in modulating the efficiency versus safety trade-off with height (Domec *et al.*, 2008).

The analysis of TEM micrographs revealed that embolism resistance was negatively correlated with torus thickness. Roots showed relatively thick tori, and tended to be more vulnerable to air-seeding than stems (Fig. 5a). This relatively strong trend was unexpected. In angiosperms, thinner pit membranes are usually more porous than thicker membranes; a trend that should be paralleled by thinner membranes being associated with greater vulnerability to embolism (Jansen *et al.*, 2009). However, air-seeding in torus–margo pits is thought to depend on factors different from those in intervessel pits (Sperry & Tyree, 1990; Hacke *et al.*, 2004). It is conceivable that a thinner torus is more flexible and hence better able to adjust its shape to the pit border and to seal the aperture. This could be important if the surface of the pit chamber is somewhat irregular, for example owing to the presence of warts. If true, this raises the question why thinner tori are not universally selected for. A possible answer is that larger pits require thicker tori to minimize the deformation of the aspirated torus, which could lead to the exposure of margo pores and hence air-seeding. Our SEM and TEM observations suggest that tori are somewhat flexible and that they can sometimes bend (Figs 1a–c, 2d). It is therefore likely that torus thickness is an adaptive parameter, and that it should be adjusted to other parameters, including the size of pits. An alternative explanation of the data shown in Fig. 5a is that torus thickness covaries with another, yet unidentified parameter that is more causally related to air-seeding. This interpretation is supported by findings in Cupressaceae, in which thicker tori appear to be associated with more *resistant* xylem (J. Pittermann *et al.*, unpublished). In addition, variation in torus thickness across conifer species could reflect developmental differences, especially with respect to a differential amount of matrix removal in mature pit membranes after autolysis (Dute, 1994; Sano *et al.*, 1999). Complete removal of matrix material from the pit membranes has been reported in *Metasequoia glyptostroboides* and *Ginkgo biloba*, while the torus remains largely unaffected in *Abies firma* (Dute, 1994; Dute *et al.*, 2008). This could be explained by a difference in chemical composition of the torus or a difference in autolytic enzymes (Dute *et al.*, 2008).

The use of TEM in conjunction with hydraulic measurements revealed another link between pit anatomy and embolism resistance. The depth of the pit chamber (or the distance between pit borders) increased with embolism resistance (Fig. 5b). Root tracheids tended to show deeper pit chambers than stem tracheids. The depth of the pit chamber is proportional to the distance the pit membrane can deflect until aspiration occurs. Increasing this distance at a given scaling of D_M, D_T and D_A increases the pit membrane strain and the potential for rupture of margo microfibrils. We therefore expect this relationship to be confirmed in other taxa as well. A likely advantage of a deeper pit chamber is that it will facilitate water flow – a hypothesis which is supported by Fig. 6b.

Tracheid dimensions were less suitable for explaining variation in embolism resistance than pit structure. Significant correlations between tracheid dimensions and P50 existed within

roots, but not within stems (with the exception of A_T, Fig. 7c). The lack of a correlation in stems may be caused by several factors. First, there was only a small range of average tracheid size in our stem samples. Second, branch xylem often exhibits structural heterogeneity because of the presence of compression wood and latewood, which are known to have altered relations between transport efficiency and safety (Domec & Gartner, 2002; Mayr & Cochard, 2003). Not only were correlations with P50 more apparent in roots than in stems, tracheids in root also showed larger pits (Figs 1, 2) and wider tracheids (Fig. 7a) at a given P50 than tracheids in stems. At the same P50, tracheids in roots were also longer (Fig. 7b) and had greater A_P (Fig. 7c) than stem tracheids. All of these differences will contribute to greater conductivities of roots at a given air-seeding pressure. Hence, stem xylem seemed less optimized in the light of a trade-off between safety and efficiency. This is in agreement with the fact that mechanical strength is more important for trunk and branch wood than for the wood of smaller lateral roots.

The data shown in Fig. 7c provides no support for the validity of the pit area hypothesis in conifer xylem. In a previous survey covering various conifer families (Pittermann *et al.*, 2006a), a correlation between P50 and A_P was found in stems, but not in roots. Here we found a relatively weak trend in roots and no correlation in stems. This inconsistency seems symptomatic of the lack of a causal link between P50 and A_P in conifer tracheids. Pit structure appears to be more closely related to differences in embolism resistance than tracheid diameter and A_P. This also follows from a related study on conifer species of the boreal forest, which revealed that tracheid diameter and embolism resistance vary independently in shaded versus open-grown saplings (A. Schoonmaker *et al.*, unpublished).

At the tissue level embolism resistance increased with increasing wood density (Fig. 8a) and at the cellular level this trend was paralleled by an underlying increase in tracheid wall reinforcement (Fig. 8b). The $(t/b)_h^2$ is related to how much bending stress a double wall dividing an air-filled from a water-filled conduit can withstand (Hacke *et al.*, 2001; Sperry, 2003). While minimum values of tracheid wall thickness and wood density have been shown to scale with embolism resistance in roots and stems of Pinaceae and Cupressaceae (Hacke *et al.*, 2001, 2004; Pittermann *et al.*, 2006b), densities and thickness-to-span ratios are often greater than what would be expected just from the perspective of cohesion-driven water transport (Mayr *et al.*, 2006; Pittermann *et al.*, 2006b), which reduces the predictive power of these parameters.

Tracheid dimensions (diameter, length, surface area and pit area) explained at least 90% of the variation in K_S when stem and root samples were pooled (Fig. 9). At the same D, conifer xylem had K_S values that were comparable to those found in the angiosperm dataset of Hacke *et al.* (2006), and in some cases were even higher. The high transport efficiency of tracheid-based xylem resulted from the high conductivity of torus–margo pits (Pittermann *et al.*, 2005), the fact that conifer wood contains more conduits per area than angiosperm wood and high pit fractions, which minimize end wall resistivity. The mean F_P of all samples was 11.4 ± 2.6% (mean ± SD), compared with only 6.4% in angiosperms (Hacke *et al.*, 2006) and 8.6% in the conifer dataset of Pittermann *et al.* (2006a). In contrast to a previous study (Pittermann *et al.*, 2006a), we observed an increase of F_P with D (data not shown). Domec *et al.* (2006) also found a higher F_P in earlywood tracheids of roots compared with branches. The increase of F_P in wider tracheids is in accord with the manner in which D changed with K_S. The slope of the increase in D with K_S was 0.32 (Fig. 9a) rather than the slope of 0.5 predicted by the Hagen–Poiseuille equation ($P < 0.001$). Hence, K_S showed an even greater increase with D than would be expected from conduits with a constant end wall limitation. This greater than expected increase of K_S occurred despite relatively modest increases of L with D (Fig. 10). The regression slope of the allometric scaling of D with L was 0.77, which is similar to the value of 0.87 found in recent studies on conifers (Pittermann *et al.*, 2006a; Sperry *et al.*, 2006). A re-evaluation of Bannan's survey of earlywood tracheid dimensions (Bannan, 1965, his Table IV) yields a SMA regression slope of 0.74. Available data therefore suggests that the increase of L with D is smaller in conifer tracheids than in vessels (Hacke *et al.*, 2006). A relatively small increase of L with D in tracheids is probably a reflection of the inherent length constraint on conifer tracheids. Short tracheids seem to be at least in part related to the dual function of tracheids in providing transport and structural support to the plant (Pittermann *et al.*, 2006b).

In conclusion, the use of SEM and TEM allowed us to analyse with greater accuracy than with LM how variation in pit anatomical properties relates to water transport. Trade-offs in hydraulic function were influenced by both tissue level changes in tracheid allometry and by pit level differences. While variation in K_S could be explained to a large degree by differences in tracheid dimensions and pit area, variation in embolism resistance was linked with torus thickness and pit chamber depth in the three species studied. This suggests that bordered pits in tracheids have the potential to provide an adaptive trait in the hydraulic safety mechanism of conifers and to drive ecological differences between taxonomic groups. However, more work is required to evaluate whether these correlations exist in other taxonomic groups and whether they are expressions of a causal link. More information on the mechanical properties of conifer pit membranes is also required to further improve our understanding of how pit structure relates to function.

Acknowledgements

U.H. acknowledges support from the Canada Research Chair program and the Canada Foundation for Innovation. S.J. acknowledges financial support from the Natural Environment Research Council (NERC, NE/E001122/1) and thanks A. Pletsers (RBG, Kew) for technical assistance with the preparation of SEM and TEM samples.

References

Alder NN, Pockman WT, Sperry JS, Nuismer S. 1997. Use of centrifugal force in the study of xylem cavitation. *Journal of Experimental Botany* **48**: 665–674.

Bannan MW. 1965. The length, tangential diameter and length/width ratio of conifer tracheids. *Canadian Journal of Botany* **43**: 967–984.

Bauch JW, Liese W, Schultze R. 1972. The morphological variability of the bordered pit membranes in gymnosperms. *Wood Science and Technology* **6**: 165–184.

Chaffey NJ. 2002. *Wood formation in trees: cell and molecular biology techniques*. London, UK: Taylor and Francis.

Cochard H, Lemoine D, Dreyer E. 1999. The effects of acclimatization to sunlight on the xylem vulnerability to embolism in *Fagus sylvatica* L. *Plant, Cell & Environment* **22**: 101–108.

Domec JC, Gartner BL. 2002. How do water transport and water storage differ in coniferous earlywood and latewood? *Journal of Experimental Botany* **53**: 2369–2379.

Domec JC, Lachenbruch B, Meinzer FC. 2006. Bordered pit structure and function determine spatial patterns of air-seeding thresholds in xylem of Douglas-fir (*Pseudotsuga menziesii*; Pinaceae) trees. *American Journal of Botany* **93**: 1588–1600.

Domec JC, Lachenbruch B, Meinzer FC, Woodruff DR, Warren JM, McCulloh KA. 2008. Maximum height in a conifer is associated with conflicting requirements for xylem design. *Proceedings of the National Academy of Sciences, USA* **105**: 12069–12074.

Dute R, Hagler L, Black A. 2008. Comparative development of intertracheary pit membranes in *Abies firma* and *Metasequoia glyptostroboides*. *IAWA Journal* **29**: 277–289.

Dute RR. 1994. Pit membrane structure and development in *Ginkgo biloba*. *IAWA Journal* **15**: 75–90.

Hacke UG, Sperry JS, Ewers BE, Ellsworth DS, Schäfer KVR, Oren R. 2000. Influence of soil porosity on water use in *Pinus taeda*. *Oecologia* **124**: 495–505.

Hacke UG, Sperry JS, Feild TS, Sano Y, Sikkema EH, Pittermann J. 2007. Water transport in vesselless angiosperms: conducting efficiency and cavitation safety. *International Journal of Plant Sciences* **168**: 1113–1126.

Hacke UG, Sperry JS, Pittermann J. 2004. Analysis of circular bordered pit function – II. Gymnosperm tracheids with torus-margo pit membranes. *American Journal of Botany* **91**: 386–400.

Hacke UG, Sperry JS, Pockman WT, Davis SD, McCulloh KA. 2001. Trends in wood density and structure are linked to prevention of xylem implosion by negative pressure. *Oecologia* **126**: 457–461.

Hacke UG, Sperry JS, Wheeler JK, Castro L. 2006. Scaling of angiosperm xylem structure with safety and efficiency. *Tree Physiology* **26**: 689–701.

van Ieperen W, van Gelder A. 2006. Ion-mediated flow changes suppressed by minimal calcium presence in xylem sap in *Chrysanthemum* and *Prunus laurocerasus*. *Journal of Experimental Botany* **57**: 2743–2750.

Jansen SJL, Choat B, Pletsers A. 2009. Morphological variation of intervessel pit membranes and implications to xylem function in angiosperms. *American Journal of Botany* **96**: 409–419.

Kavanagh KL, Bond BJ, Aitken SN, Gartner BL, Knowe S. 1999. Shoot and root vulnerability to xylem cavitation in four populations of Douglas-fir seedlings. *Tree Physiology* **19**: 31–37.

Lancashire JR, Ennos AR. 2002. Modelling the hydrodynamic resistance of bordered pits. *Journal of Experimental Botany* **53**: 1485–1493.

Mayr S, Cochard H. 2003. A new method for vulnerability analysis of small xylem areas reveals that compression wood of Norway spruce has lower hydraulic safety than opposite wood. *Plant, Cell & Environment* **26**: 1365–1371.

Mayr S, Hacke U, Schmid P, Schwienbacher F, Gruber A. 2006. Frost drought in conifers at the alpine timberline: xylem dysfunction and adaptations. *Ecology* **87**: 3175–3185.

Panshin AJ, de Zeeuw C. 1970. *Textbook of wood technology*. New York, NY, USA: McGraw-Hill.

Pittermann J, Sperry JS, Hacke UG, Wheeler JK, Sikkema EH. 2005. Torus-margo pits help conifers compete with angiosperms. *Science* **310**: 1924–1924.

Pittermann J, Sperry JS, Hacke UG, Wheeler JK, Sikkema EH. 2006a. Inter-tracheid pitting and the hydraulic efficiency of conifer wood: the role of tracheid allometry and cavitation protection. *American Journal of Botany* **93**: 1265–1273.

Pittermann J, Sperry JS, Wheeler JK, Hacke UG, Sikkema EH. 2006b. Mechanical reinforcement of tracheids compromises the hydraulic efficiency of conifer xylem. *Plant, Cell & Environment* **29**: 1618–1628.

Rundel PW, Stecker RE. 1977. Morphological adaptations of tracheid structure to water stress gradients in the crown of *Sequoiadendron giganteum*. *Oecologia* **27**: 135–139.

Sano Y, Kawakami Y, Ohtani J. 1999. Variation in the structure of intertracheary pit membranes in *Abies sachalinensis*, as observed by field-emission scanning electron microscopy. *IAWA Journal* **20**: 375–388.

Sperry JS. 2003. Evolution of water transport and xylem structure. *International Journal of Plant Sciences* **164**: S115–S127.

Sperry JS, Donnelly JR, Tyree MT. 1988. A method for measuring hydraulic conductivity and embolism in xylem. *Plant, Cell & Environment* **11**: 35–40.

Sperry JS, Hacke UG, Pittermann J. 2006. Size and function in conifer tracheids and angiosperm vessels. *American Journal of Botany* **93**: 1490–1500.

Sperry JS, Ikeda T. 1997. Xylem cavitation in roots and stems of Douglas-fir and white fir. *Tree Physiology* **17**: 275–280.

Sperry JS, Tyree MT. 1990. Water-stress-induced xylem embolism in three species of conifers. *Plant, Cell & Environment* **13**: 427–436.

Tyree MT, Zimmermann MH. 2002. *Xylem structure and the ascent of sap*. Berlin, Germany: Springer.

Warton DI, Wright IJ, Falster DS, Westoby M. 2006. Bivariate line-fitting methods for allometry. *Biological Reviews* **81**: 259–291.

Wheeler JK, Sperry JS, Hacke UG, Hoang N. 2005. Inter-vessel pitting and cavitation in woody Rosaceae and other vesselled plants: a basis for a safety versus efficiency trade-off in xylem transport. *Plant, Cell & Environment* **28**: 800–812.